INTERFACE

royalsocietypublishing.org/journal/rsif

Research

Cite this article: Checa AG, González-Segura A, Rodríguez-Navarro AB, Lagos NA. 2020 Microstructure and crystallography of the wall plates of the giant barnacle *Austromegabalanus psittacus*: a material organized by crystal growth. *J. R. Soc. Interface* **17**: 20190743. http://dx.doi.org/10.1098/rsif.2019.0743

Received: 31 October 2019
Accepted: 11 February 2020

Subject Category:
Life Sciences–Physics interface

Subject Areas:
biomaterials, biophysics

Keywords:
biomineralization, barnacle, plate, crystallography, electron backscatter diffraction

Author for correspondence:
Antonio G. Checa
e-mail: acheca@ugr.es

Electronic supplementary material is available online at https://doi.org/10.6084/m9.figshare.c.4860666.

THE ROYAL SOCIETY PUBLISHING

Microstructure and crystallography of the wall plates of the giant barnacle *Austromegabalanus psittacus*: a material organized by crystal growth

Antonio G. Checa[1,4], Alicia González-Segura[2], Alejandro B. Rodríguez-Navarro[3] and Nelson A. Lagos[5]

[1]Departamento de Estratigrafía y Paleontología, [2]Centro de Instrumentación Científica, and [3]Departamento de Mineralogía y Petrología, Universidad de Granada, 18071 Granada, Spain
[4]Instituto Andaluz de Ciencias de la Tierra, CSIC-Universidad de Granada, 18100 Armilla, Spain
[5]Centro de Investigación e Innovación para el Cambio Climático, Universidad Santo Tomás, Santiago, Chile

AGC, 0000-0001-7873-7545

In biomineralization, it is essential to know the microstructural and crystallographic organization of natural hard tissues. This knowledge is virtually absent in the case of barnacles. Here, we have examined the crystal morphology and orientation of the wall plates of the giant barnacle *Austromegabalanus psittacus* by means of optical and electron microscopy, and electron backscatter diffraction. The wall plates are made of calcite grains, which change in morphology from irregular to rhombohedral, except for the radii and alae, where fibrous calcite is produced. Both the grains and fibres arrange into bundles made of crystallographically co-oriented units, which grow onto each other epitaxially. We call these areas crystallographically coherent regions (CCRs). Each CCR elongates and disposes its *c*-axis perpendicularly or at a high angle to the growth surfaces, whereas the *a*-axes of adjacent CCRs differ in orientation. In the absence of obvious organic matrices, this pattern of organization is interpreted to be produced by purely crystallographic processes. In particular, due to crystal competition, CCRs orient their fastest growth axes perpendicular to the growth surface. Since each CCR is an aggregate of grains, the fastest growth axis is that along which crystals stack up more rapidly, that is, the crystallographic *c*-axis in granular calcite. In summary, the material forming the wall plates of the studied barnacles is under very little biological control and the main role of the mantle cells is to provide the construction materials to the growth front.

1. Introduction

Barnacles are sessile crustaceans forming the infraclass Cirripedia. Within this group, the so-called acorn barnacles (order Sessilia) attach their shells directly to the substrate. They have a variable number of lateral calcified plates that show incremental growth, and most of them attach to the substrate directly or by means of a basal calcified plate. Acorn barnacles are essential components in present-day littoral environments for both their abundance and ubiquity [1], and due to their attached lifestyle to natural and man-made hard substrata, they are one of the most important taxa studied in biofouling research [2]. The Balanidae are an important family of acorn barnacles, with six lateral plates (except for the four-plated genus *Tetrabalanus* [3]) and a calcareous tubiferous base plate.

Despite the extensive literature on barnacles, few studies have dealt with the microstructure and crystallography of their calcified plates. The main morphological elements of the barnacle plate system are shown in figure 1. The only comprehensive microstructural studies are those of Bourget [4,5], who

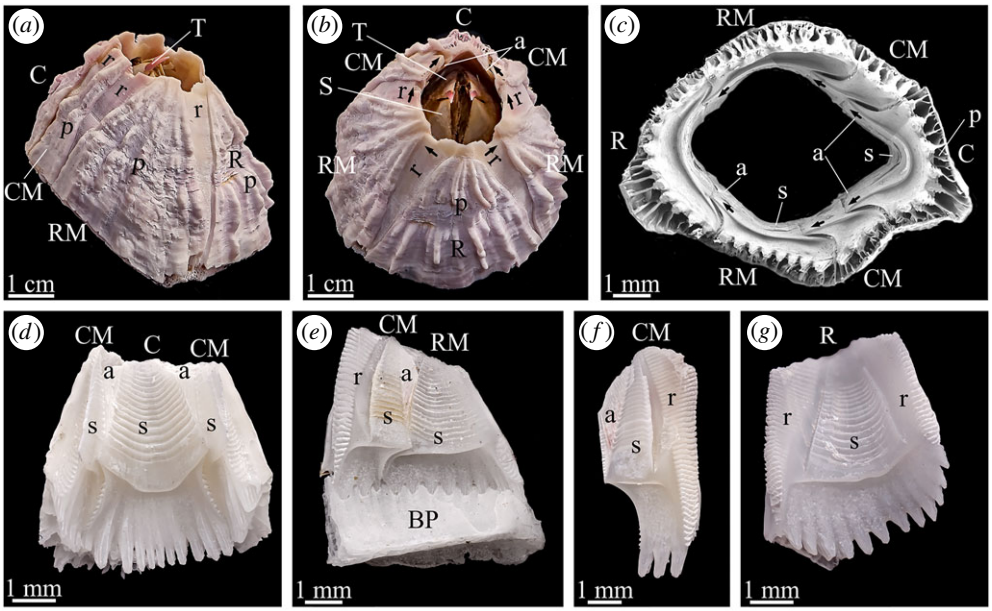

Figure 1. Wall plate arrangement and morphology in *A. psittacus*. (*a*) Right anterior view. (*b*) Anterior dorsal view. Arrows indicate the growth directions of radii. (*c*) Basal view, with base plate removed. Arrows indicate the growth directions of alae. (*d–g*) Internal views of wall plates. (*d*) Carina plus adjacent carinomarginals. (*e*) Rostromarginal and carinomarginal, attached to basal plate. (*f*) Isolated carinomarginal. (*g*) Isolated rostrum. a, ala; BP, base plate; C, carina; CM, carinomarginal; p, paries; R, rostrum; r, radius; RM, rostromarginal; S, scutum; s, sheath; T, tergum.

summarized the scarce previous knowledge and described the granular microstructure composing the interior of the plate paries and basal plate, and the fibrillar crystals forming the radius margin in several acorn barnacles, including members of the Balanidae (*Balanus balanoides*, *Amphibalanus amphitrite*). Similar granular units were also described in the giant barnacle *Austromegabalanus psittacus* [6] in both the outer and inner surfaces of the parietes and basal plate, whereas the sheath consisted of subparallel oriented lamellae, in turn, composed of small equiaxial grains. Grains plus rhomboedral crystals were also observed at the base plate of *B. albicostatus* [7]. In *B. amphitrite*, similar microstructural elements were observed in the scutum, whereas the wall plates were made of densely packed small irregular crystalline units [8]. In summary, knowledge on the microstructure of the shell plates is limited, particularly taking into account that the most comprehensive studies [4,5] were carried out with low-resolution scanning electron microscopy (SEM).

Data on the crystallography of calcified elements are particularly scarce. X-ray diffraction revealed that the crystallites of the outer surface of the plates are relatively disorganized, whereas those of the internal surface have a crystallographic fibre texture, with the *c*-axis perpendicular to the plate's internal surface [6]. Electron backscatter diffraction (EBSD) applied to the shell plates of *Balanus amphitrite* did not reveal any preferred orientation in the wall plates [9]. At the base plate, the calcite crystals' *c*-axes are perpendicular to the base plate close to the substrate and later change to become parallel to the attachment surface towards the middle of the base plate. EBSD maps obtained on the margins of the alae in the horizontal section revealed crystalline domains with complex boundaries, which elongated perpendicular to the growth margin, thus having a radial arrangement [10]. The *c*-axes of these domains display a similar distribution. Accordingly, the only three previous studies focused on different parts of the plates and showed some contradictions as to the degree of crystallographic organization of the wall plates. In summary, they do not provide a clear picture of the crystalline organization of the plates.

The wall plates of acorn barnacles are extensively calcified elements. Whether these structures, in fact, show a certain internal crystallographic organization or not is an essential aspect, in order to enable hypotheses about their growth pattern. With this aim, we have studied the ultrastructure and crystallography of the wall plates of the giant barnacle *A. psittacus* in detail by means of high-resolution SEM and EBSD. These techniques reveal a certain degree of internal organization of the material forming the wall plates, which can be explained purely by crystal growth processes taking place within the otherwise microstructurally monotonic biomaterial. This implies that, unlike other invertebrates (molluscs, brachiopods), the animal exerts little control over the formation of its shell's microstructures. Given the low diversity of microstructures found within the sessilian barnacles (see above), these conclusions can possibly be made general to the group.

2. Material and methods

2.1. Material

Specimens of the balanomorph *A. psittacus* (family Balanidae, subfamily Megabalaninae) come from Isla Santa María, close to Antofagasta (*ca* 23° S, northern Chile). All specimens were sampled alive.

2.2. Optical microscopy

Two specimens of *A. psittacus* were fixed in 2.5% glutaraldehyde, with 0.1 M cacodylate buffer, pH 7.4, for 2 days, and later kept in cacodylate buffer at 4°C. Two specimens of *A. psittacus* were dehydrated and embedded in Technovit 7200 VLC methacrylate-based resin in five steps. The first three steps were combinations of ethanol (Et) and progressively increasing proportions of Technovit (T) (30T : 70Et; 50T : 50Et; 70T : 30Et); the last two steps

consisted only of Technovit 7200 VLC. The samples were subsequently polymerized. The embedded tissues were sectioned to a thickness of 50 µm using the cutting band system EXAKT 300CL. One of the specimens was sectioned perpendicular to the growth axis, while the other was sectioned parallel to this axis. The sections were ground with a precision micro-grinding system EXAKT 400 C, and stained with toluidine blue to reveal the organic phase. This entire process was carried out in the Andalusian Centre of Nanomedicine and Biotechnology (BIONAND, Málaga, Spain).

Other specimens were oven-dried and cleaned with commercial bleach (approx. 5% active chlorine for 3–5 min). They were embedded in polyester resin (Vosschemie GTS), cut and thinned down with silicon carbide powder to transparency (approx. 30 µm). Sections were photographed with a Leica DM1000 LED optical microscope, equipped with a Leica DFC295 camera, belonging to the Department of Stratigraphy and Paleontology of the University of Granada (UGR), Spain.

2.3. Scanning electron microscopy

Ultrasonicated complete specimens, as well as disarticulated wall plates (cleaned by immersion in commercial bleach, approx. 5% active chlorine, for 30–60 min), fractured plates (also cleaned with commercial bleach, for 4–5 min) and polished sections (previously etched for 2–3 min with 4% EDTA) were prepared for SEM observation. All samples were carbon-coated (Emitech K975X carbon evaporator) and observed in the field emission SEM (FESEM) equipments Zeiss Auriga and FEI QemScan 650 F of the Centre for Scientific Instrumentation (CIC) of the UGR.

2.4. Electron backscatter diffraction

Four wall plates of two specimens of *A. psittacus* were embedded (Vosschemie GTS polyester resin) and sectioned in horizontal and vertical directions, taking care to cut precisely through the main structural elements (parietes, radii, sheaths and alae). Sections were polished on diamond-impregnated discs (Struers Planopol 2 polishing machine) with grit sizes 3, 1 and 0.75 µm, followed by final polishing with colloidal silica. Sample charging was reduced by coating with a thickness of 2 nm of carbon in a BAL-TEC MED 020 electron beam evaporator. EBSD analyses were carried out in a Zeiss Auriga CrossBeam Workstation equipped with an Oxford Instruments Nordlysnano EBSD detector of the CIC (UGR). For maps made on polished sections, the machine was operated at 10 kV, and the step size was set between 2 µm and 30 nm, depending on the desired resolution. The exact areas mapped on the samples are shown in electronic supplementary material, figure S1. Data were post-processed with the analysis software HKL CHANNEL5 (Oxford Instruments) and is presented in the form of orientation colour maps and pole figures. No grain dilation or averaging was applied. Multiples of uniform density (MUD) values have been calculated for sets of 100 and 001 pole densities. These values represent the strength of the clustering of poles, relative to that of a random distribution, or, in other terms, they are proportional to the degree of co-orientation of crystals (e.g. [11]). All instruments are housed in the CIC (UGR).

3. Results

3.1. Morphology, structure and growth surfaces of wall plates

For the description of the wall plates and their structures, we follow the terminology provided by the authors in [12–15]. The wall is made by six plates: an anterior rostrum, two rostromarginals, two carinomarginals and a posterior carina (figure 1*a–c*). Apart from the paries, the rostrum bears two lateral radii. The rostromarginal and carinomarginal plates bear one radius extending in the direction of the carina, and the carina has no associated radius. Internally, all plates have a sheath, which extends from the ventral margin towards the dorsum. The sheath may extend laterally into alae. The sheath of the carina has two alae (figure 1*d*), while those of the rostromarginals and carinomarginals have only one ala (figure 1*d–f*), and the sheath of the rostrum has no alae (figure 1*g*). All alae grow in the direction of the rostrum (arrows in figure 1*c*), and their growth compensates for the carinal-ward growth of the radii (arrows in figure 1*b*).

In addition to the wall plates, *A. psittacus* bears four opercular plates, two terga, with prominent beaks, and two scuta (figure 1*a,b*). Attachment to the substrate is accomplished by means of a tubiferous basal plate, which consists of an internal (i.e. in contact with the main body cavity) layer of wide primary tubes, and an external layer of subsidiary tubes.

Each wall plate is defined by three main growth margins: (i) the basally growing margins of the parietes, (ii) the laterally growing margins of the radii, and (iii) the dorsally to laterally continuous growing margin of the sheath–ala complex.

3.1.1. Basal growth margin of the paries

At this margin, there is a relatively complex system of structures composed of the outer and inner lamina, together with primary septa, which extend perpendicularly to and between the two laminae (figure 2*a,b*). In this way, they delineate the entrance to the longitudinal canals (primary canals), which run dorsoventrally across the paries interior (figure 2*b*). The primary septa directly interlock, in a one-to-one correspondence, with the radially oriented primary tubes of the base plate (figure 1*e*). There are also secondary septa intermediate between the primary septa, which extend for a short distance from the outer lamina (figure 2*a*). Towards the inner lamina, there are denticles diverging laterally from the primary septa (figure 2*a,b*). From the edges of both the primary septa and the denticles, the septal surface invaginates, forming a series of troughs that extend in the lateroventral direction (figure 2*a,b*). With growth, new material is added to both the dorsal surfaces of the septa and to the interior surfaces of the longitudinal canals. In this way, the formerly laid down primary septa become progressively integrated within the paries. Their non-denticulated portions thicken to form the longitudinal septa, which separate the longitudinal canals running dorsoventrally along the paries interior (figure 2*c*). The denticulated portions of the primary septa become embedded within the inner lamina, producing the so-called interlaminate figures [12] (figure 2*c–e*). Rather diffuse growth lines associated with the interlaminate figures show how the acute reliefs of the septa and denticles become progressively attenuated with further growth (figure 2*d,e*). The progressive infilling of the longitudinal canals takes place preferentially from the outer lamina towards the canal interior, as indicated by the distribution of growth lines (figure 2*d*).

3.1.2. Lateral growth margin of the radius

The paries material is continuous into the radius, with the difference that the latter is characterized by lateral (carinal-ward) growth, instead of vertical (dorsal) growth. In external view, radii become wider in the ventral direction (figure 1*a,b*).

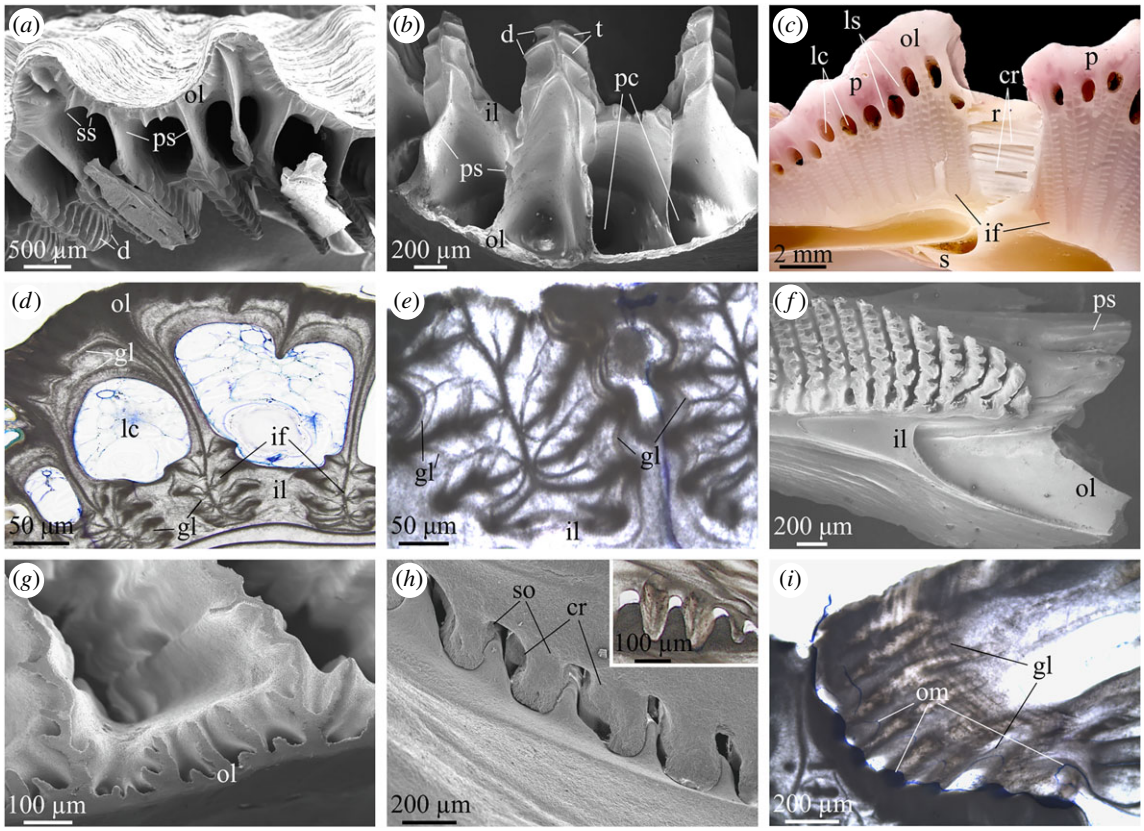

Figure 2. Structures found in the paries and radius. (*a*) Basal view of the paries growth margin. Some fragments of the basal plate remained between the primary septa upon detachment. (*b*) Basal view of another specimen showing details of the primary septa and denticles. (*c*) Horizontal section across the contact between two plates showing the structures integrated within the paries and radius. The interlaminate figures and radius crenulations are to be noted. (*d*) Horizontal section through the wall of the paries, with indication of the main elements. The distribution of growth lines around the longitudinal canals is clearly asymmetric. Note organic infillings (in blue) within the longitudinal canals. (*e*) Detail of an interlaminate figure (horizontal section) showing the distribution of growth lines around the sectioned primary septum and denticles (thick dark lines). (*f*) Crenulations of the basal part of the growth margin of radius. Note their dendritic outlines. (*g*) Detail of the dendritic features observed in the growth margin of the radius. (*h*) Interlocking system at the radius–paries junction. The inset is an optical view of a section through a similar interlocking system. Note the void spaces at the interior of the sockets. (*i*) Horizontal section through the contact paries–radius. There are organic membranes (stained in blue) both at the very contact and integrated within the radius. (*a,b,f,g,h*) are SEM images; (*c*) is an optical image; (*d,e*), the inset in (*h*), and (*i*) are transmitted light images, where the organic membranes are stained with toluidine blue. cr, crenulation; d, denticle; gl, growth line; if, interlaminate figure; il, inner lamina; lc, longitudinal canal; ls, longitudinal septum; ol, outer lamina; om, organic membrane; pc, primary canal; p, paries; ps, primary septum; r, radius; s, sheath; so, socket; ss, secondary septum; t, trough.

Their carinal growth margins directly abut the rostral margins of the adjacent plate parietes. The radius margin develops a series of horizontal crenulations with dendritic outlines separated by relatively deep troughs (figure 2*f,g*), which interlock with a series of less prominent complementary crests and troughs of the rostral margin of the paries (figure 2*h*). With lateral growth, the radius crests generate a series of horizontal elements, which can be seen either in section (figure 2*c*; electronic supplementary material, figure S1, Sample 3) or by transparency when looking from the internal shell surface (figure 1*e–g*). Growth lines observed on horizontal sections indicate that local growth directions change at every minor nook corresponding to different-order branches of the dendritic margins of the crenulations (figure 2*i*). At the paries margins opposing the radius growth margins, some diffuse growth lines can be found within the crests, but not within the troughs (figure 2*h* inset).

3.1.3. Growing margin of the sheath–ala complex

The sheath or sheath–ala complex is secreted internally to the paries and radius (figure 3*a*). It is formed by the internal layer [4], which gives it a more translucent aspect than the material forming the paries–radius. In the vertical section, the dorsal margin of the sheath is marked by a pronounced ventrally directed sinus which later extends to the lap of the sheath (figure 3*a*). Dorsoventral (vertical) sections of the sheath reveal the presence of growth lines separated by widely spaced and continuous organic membranes associated with thick dark growth increments (possibly due to greater richness in intracrystalline organic content), which run up to the basal limit of the internal layer (figure 3*a,b*). Since these membranes conform tightly to the growth surface of the sheath and to the tracing of growth lines (figure 3*b*), they should correspond to major growth episodes of unknown nature. These membranes are also found within the radii (figure 2*i*) and, sometimes, within the longitudinal canal infillings [16].

Both in section and in internal view of the plates, the growth margin of the sheath is found dorsally at a short distance from the dorsal edge of the sheath (figure 3*a,c*), and is continuous with the growth boundaries of both of the ala in the rostral direction and the internal surface of the radius in the carinal direction (figure 3*c*). The boundary between

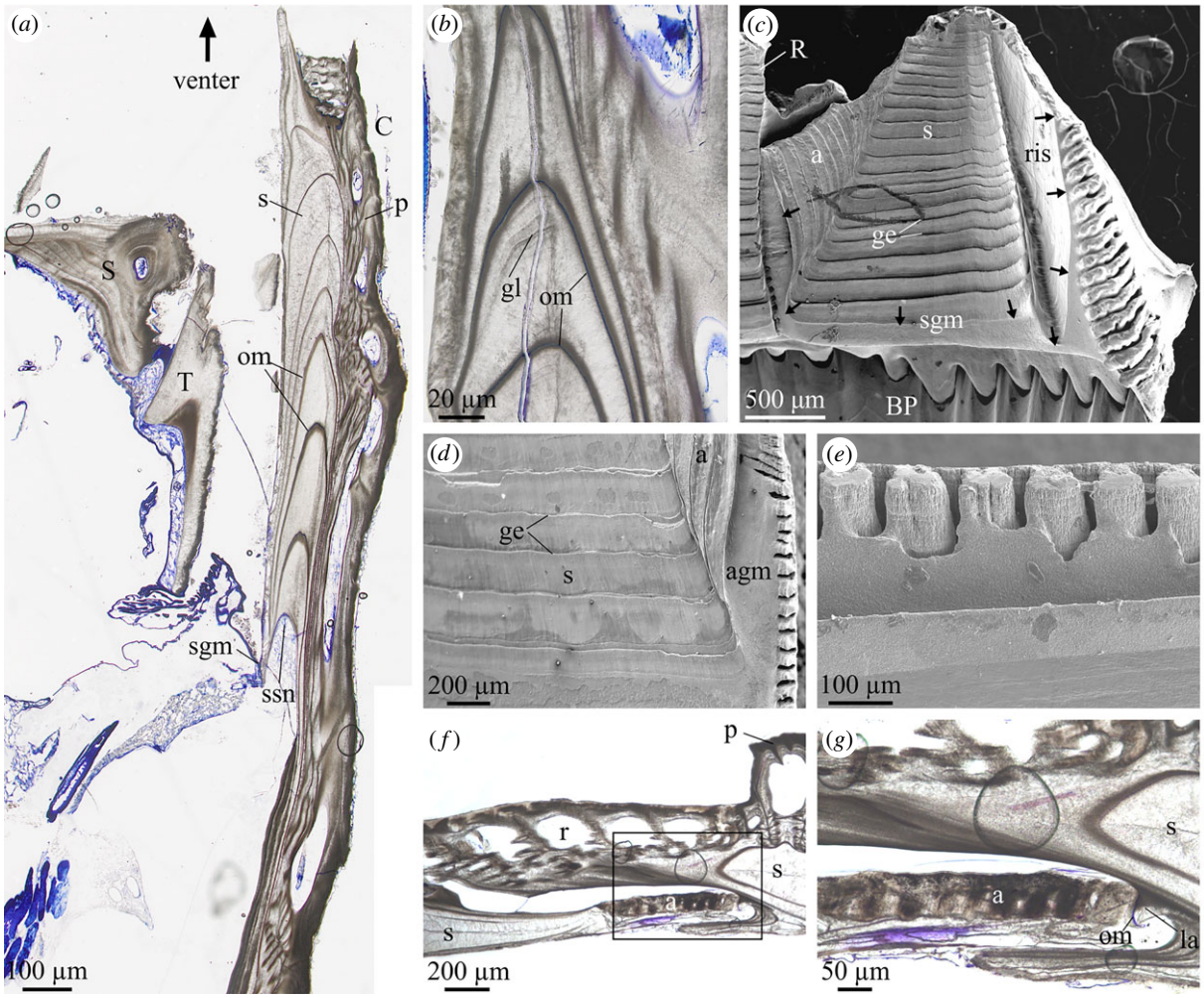

Figure 3. Structures found in the sheath and ala. (*a*) Vertical section through the carina, scutum and tergum of a fixed specimen. The distribution of parallel organic membranes within the sheath is noteworthy. All organic tissues are stained in blue. (*b*) Distribution of organic membranes (thin blue lines) and growth lines (thin and coarse dark lines) within the sheath interior (vertical section). (*c*) View of the interior surface of a rostromarginal plate. The growth front (arrows) is continuous throughout the ala, sheath and internal surface of the radius. (*d*) Partial view of the sheath and ala, including its growth margin. (*e*) View of the growth margin of the ala, showing the pillar-like aspect of the crenulations. (*f*) Horizontal section through the contact between the sheath and ala of two abutting plates. (*g*) Detail of the contact between the ala and the longitudinal abutment developed at the radius interior. Note the organic membrane (stained in blue) between the two structures. (*a,b,f,g*) are transmitted light optical images, stained with toluidine blue; (*c–e*) are SEM images. a, ala; agm, ala growth margin; BP, base plate; C, carina; ge, major growth episodes; gl, growth line; la, longitudinal abutment; om, organic membrane; p, paries; R, rostrum; r, radius; ris, radius internal surface; S, scutum; s, sheath; sgm, sheath growth margin; ssn, sheath sinus; T, tergum.

sheath and ala or alae is marked by a neat change in orientation of the otherwise continuous growth lines, from parallel to the dorsal (lower) margin of the sheath to parallel to the dorsoventral margin of the ala (figures 1*d–f* and 3*c,d*). When the sheath surface is well preserved (particularly in juveniles), there are periodically spaced high-relief growth markings (figure 3*c,d*), which are continuous into the ala. Since the sheath–ala surface is exposed during the animal's life, these surface structures deteriorate as the animal ages. These markings are the surface manifestation of the major growth episodes observed in dorsoventral sections (figure 3*a,b*). The alae develop narrow growth margins with incipiently dendritic crests and deep, narrow troughs, thus forming a pillar-like system (figure 3*d,e*). In the horizontal section, the difference between sheath and ala is clear, since the latter is made of a less translucent material with neat growth lines (figure 3*f*), which correspond to the dorsoventral growth lines observed on the surface (figure 3*c,d*). The ala growth margin connects directly with the longitudinal abutment, a ledge of the interior of the adjacent plate radius, immediately adjacent to the sheath (figure 3*g*).

3.2. Microstructures

We have identified two different microstructures in the wall plates of *A. psittacus*. The most common is by far a microstructure composed of calcite grains, which change from irregular to rounded to rhombohedral (figure 4*a–e*). Their sizes range from less than 0.5 µm to almost 10 µm, in the case of large rhombohedra (figure 4*d,e*). The interior surfaces of the plates are characterized by relatively small grains (figure 4*a*), whereas the largest sizes have been observed at the centres of the troughs formed between both the primary septa and the denticles of the dorsal area of the paries (figures 2*b* and 4*e*), and the branches of the dendrites developed at the carinal growth margins of the radii (figure 2*g*). According to their morphology, calcite grains with a rhombohedral morphology are bounded by {104} faces. It is notable

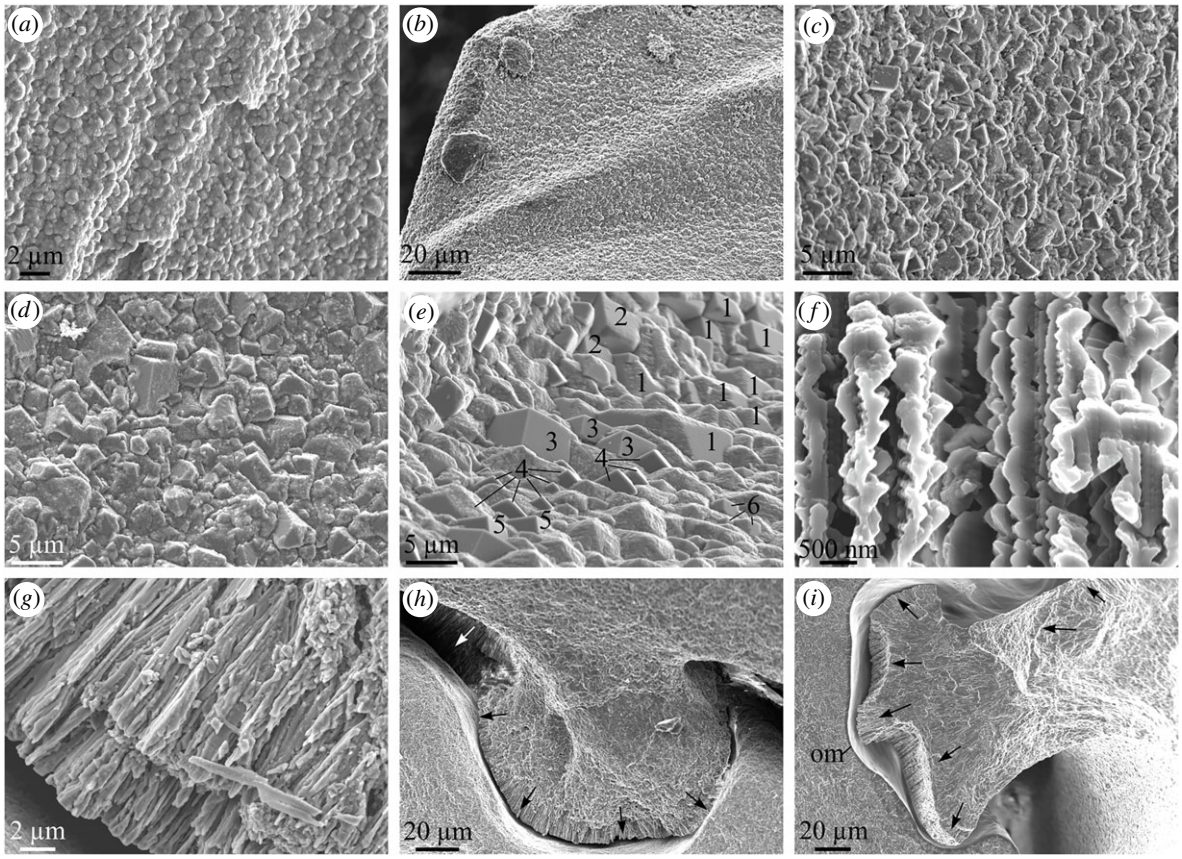

Figure 4. Microstructures of the wall plates. (*a*) Calcite grains observed at the growth surface of the plate interior, dorsal to the sheath. (*b*) Growth surface of a primary septum studded with calcite grains. (*c*) Detail of the calcite grains observed in (*b*). (*d*) Calcite grains (many of them rhombohedra) observed on the growth surface of a plate, close to the basis. (*e*) Grains of the growth surface of a trough between primary septum and denticles (figure 2*b*). The same numbers indicate evenly oriented rhombohedra. (*f*) Detail of the fibres within the pillar-like element of the alar margin. The fibre margins are typically serrated. (*g*) Fibrous microstructure of the interior of a crenulation of the radius margin. (*h*) Crenulation of a radius. The arrows indicate the orientations of the fibres at particular positions of the crenulation. (*i*) Detail of a trifurcate crenulation. Note that fibres change their orientations (arrows) to remain perpendicular to the changing morphology of the crenulation margin. The paries surface is carpeted with an organic membrane. All SEM images. om, organic membrane.

that the forming or complete {104} faces are much smoother than other types of surfaces, which are markedly nanogranular, as in other biominerals [17]. Grains clearly interpenetrate with each other (figure 4*d*,*e*), and when the rhombohedra are neatly developed, clusters of coherently oriented crystals can be recognized (figure 4*e*).

There is a second type of microstructure which is only observed within (1) the pillar-like dendritic crests of the ala growth margins (figures 3*d*,*e* and 4*f*) and (2) the dendritic crests of the radius growth margins (figures 2*f*,*h*,*i* and 4*g*–*i*). These structures are composed of thin fibres (less than 0.5 µm), which are ineluctably perpendicular to the growth surfaces (figure 4*f*–*i*). Fractures through the dendritic crenulations of the radius margins show that the fibres are able to change their orientations over short distances to fulfil the latter condition (figure 4*h*,*i*; electronic supplementary material, figure S2). The fibres tend to have straight edges in case (2) (figure 4*g*), but serrated edges in case (1) (figure 4*f*), which are suggestive of rhombohedral outlines. It is to be recalled that both the pillar-like extensions of the ala growth margins and the tips of the dendritic crenulations developed at the radius growth margins partly grow directly in contact with acellular membranes [16] (figures 2*i*, 3*g* and 4*h*,*i*; electronic supplementary material, figure S2). We have not been able to recognize a similar microstructure at the edges of the primary septa and denticles, where growth is also in contact with similar organic membranes, due to the extreme thinness of these structures.

3.3. Crystallography

Analyses made on sections of the sheath and paries (interlaminate figures) (figures 5 and 6, respectively) provided relatively complete maps, whereas those made on sections of the radius were of poorer quality (figure 7), possibly due to the small crystallite size. The map on the horizontal section of an ala retrieved a very small percentage of indexation (electronic supplementary material, figure S3), possibly for similar reasons. The exact positions of the maps on the sectioned samples can be checked in electronic supplementary material, figure S1.

The colour maps of the sheath (both horizontal and vertical sections) reveal the existence of regions or domains with a coherent crystallographic orientation (crystallographically coherent regions, here abbreviated as CCRs), which elongate approximately perpendicular to the growth episodes marked by internal organic membranes (see above) (figure 5*a*–*c*). In figure 5*a*, there is a neat divide in hue above and below the elongation axis, which is due to the crystals above having their *c*-axes inclined (so that their colours correspond to more internal areas within the orientation colour key), while the crystals below have their *c*-axes horizontal

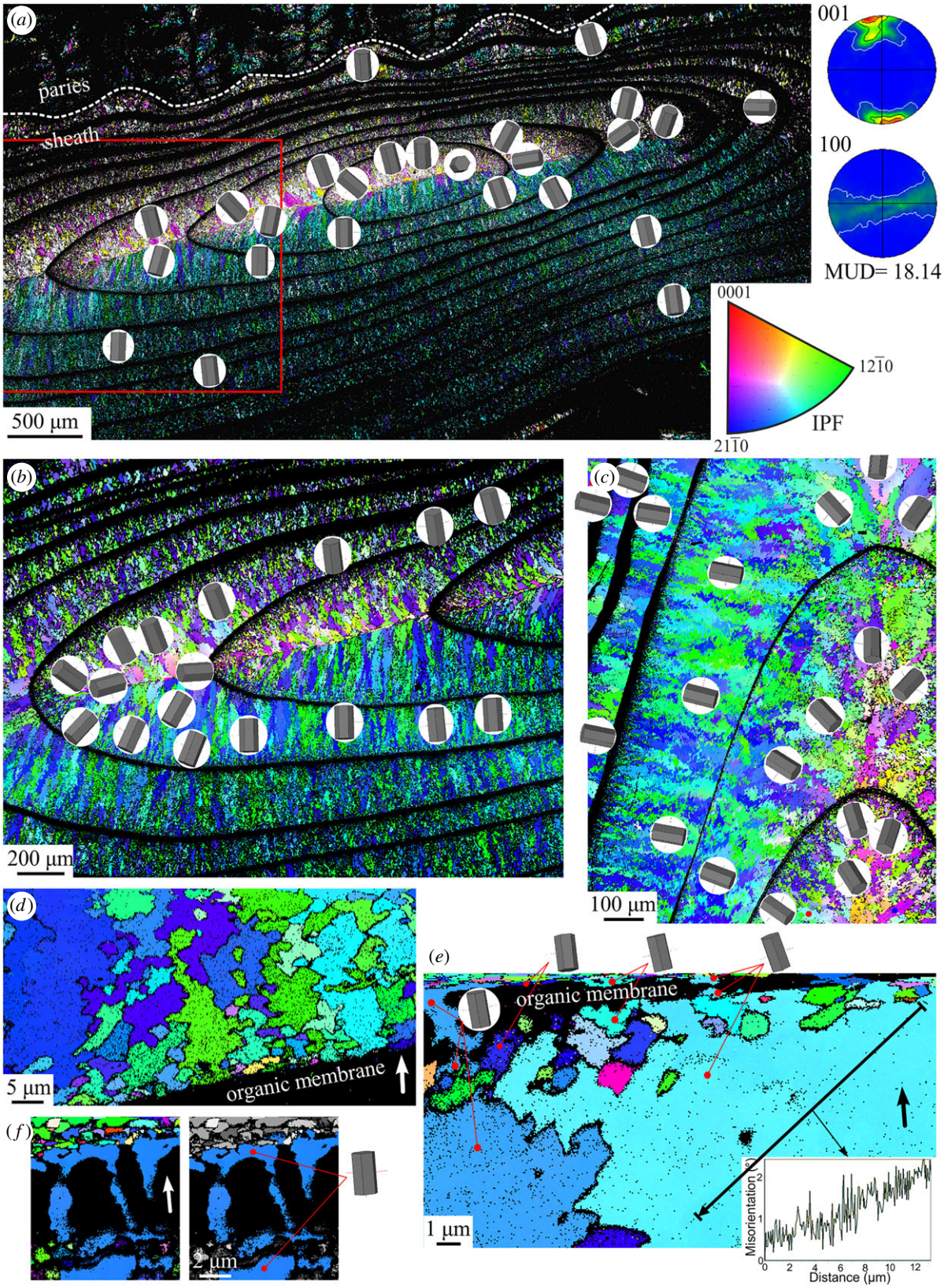

Figure 5. EBSD analysis of the sheath. (*a*) General map of a horizontal section of the sheath, with paries at the top (approximate boundary indicated). There is a general arrangement with CCRs elongating perpendicular to the growth episodes (thick black lines). Unit cells indicate that their *c*-axes are parallel to the direction of elongation and perpendicular to the growth episodes. The 001 pole figure shows a preferential distribution of the *c*-axes more or less perpendicular to the axis of elongation of the flat ovals delineated by the growth episodes. The 100 poles indicate no preferential orientation of the *a*-axes. The growth direction of the CCRs in this kind of section is towards the more internal growth episodes (i.e. centripetal). IPF, inverse pole figure (orientation colour key), valid for all maps. (*b*) Detailed map of an area partly shown in (*a*) (framed). (*c*) Vertical section of the sheath. Unit cells at particular positions are shown in (*b*,*c*). In both maps, the crystallographic domains and the *c*-axes of unit cells are perpendicular to the growth episodes. (*d*) Detail of CCRs in a horizontal section of the sheath. Their outlines are extremely irregular. (*e*) Map across an organic membrane (in black, top of image). Some CCRs extend across the membrane (as indicated by the unit cells). The misorientation profile across the big light blue CCR indicates small but persistent changes in orientation. (*f*) Detail of a CCR (blue) crossing an organic membrane (black areas). The CCR has been isolated in the right image. The thick black lines in (*a*–*c*) are organic membranes of the kind shown in figure 3*a*,*b*, and mark growth episodes. Arrows in (*d*–*f*) indicate the growth direction.

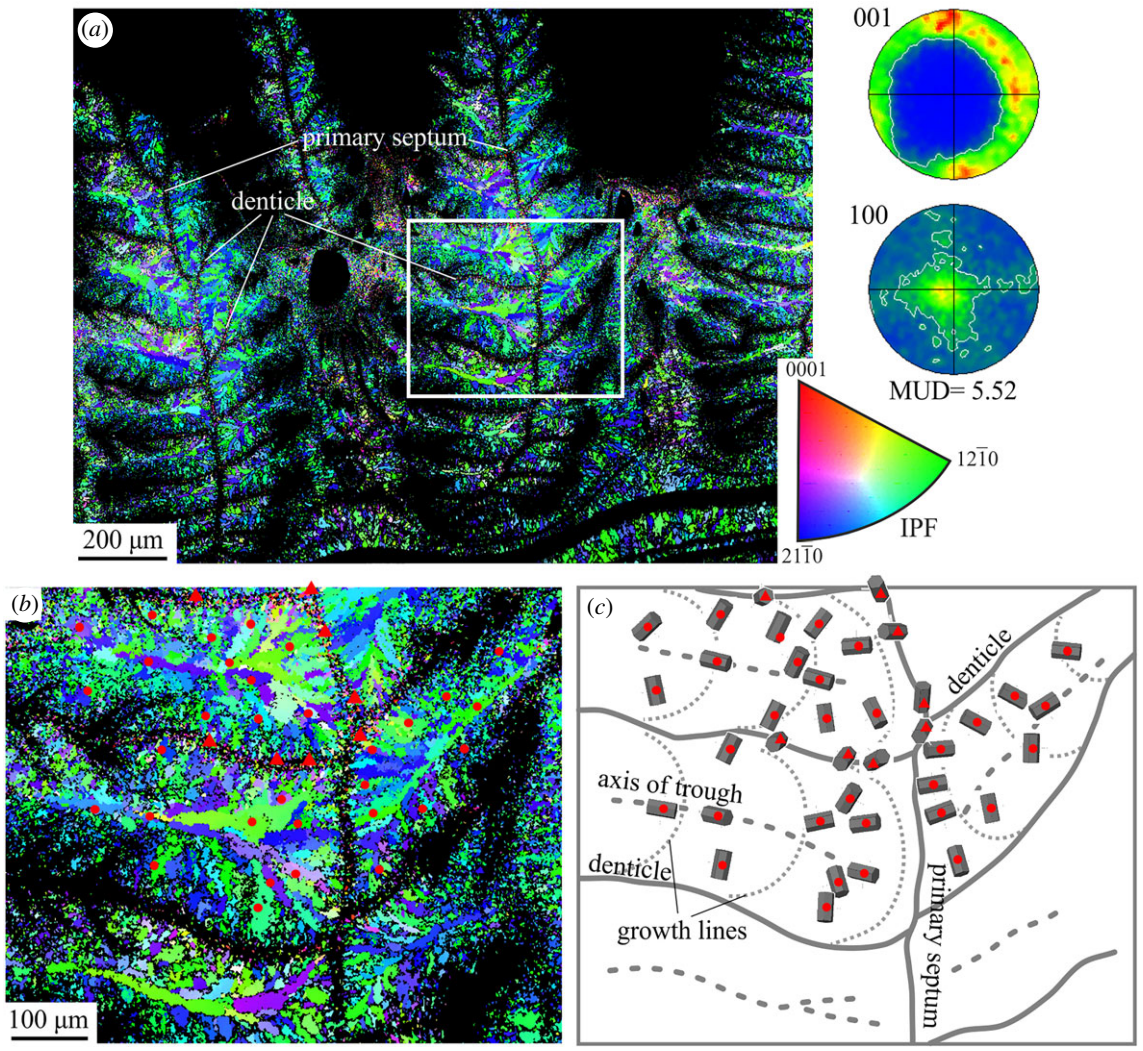

Figure 6. EBSD analysis of the interlaminate figures of the paries. (*a*) Large-scale map of several interlaminate figures. The 001 pole figure indicates that the *c*-axes are more or less in plane but without any preferential orientation. The *a*-axes (100 pole figure) can take almost any orientation. IPF (inverse pole figure) is the orientation colour key. (*b,c*) Detailed map of the area framed in (*a,b*) and sketch of the main features found within that area (*c*). The CCRs elongate perpendicularly to the primary septum and denticles and parallel to the axis of the troughs. Unit cells indicated with dots tend to orient with their *c*-axes perpendicular to the growth lines (estimated from images like those in figure 2*d,e*). Unit cells marked with triangles correspond to crystals within the edges of the primary septum and denticles, and their *c*-axes are at a high angle to the surface. The positions of the unit cells are also indicated in (*b*) with dots and triangles.

(corresponding to colours closer to the lower curved margin of the orientation colour key). Detailed maps reveal the complex irregular outlines (sometimes dendritic) of the CCRs (figure 5*b–d*). These outlines contain frequent angular-shaped features, indicative of rhombohedra outlines (figure 5*d,e*). The CCRs have extremely varied dimensions, from a few to more than a hundred micrometres in length (figure 5*b–e*). Taking into account the relatively reduced sizes of the grains observed at the plate's internal growth surfaces (figure 4*a–c*), every CCR must be a cluster of many co-oriented crystals. Accordingly, CCRs are a level of organization above the individual crystals. When we plot the crystal unit cells (figure 5*a–c,e*), it becomes clear that the *c*-axes of crystallites are always perpendicular to the growth surfaces. All the green to blue CCRs in figure 5 have *c*-axes more or less in-plane, and the differences in colour indicate differences in the orientation of the *a*-axes. Misorientation profiles within CCRs show continuous changes in the crystalline orientation of crystals, but of relatively small values (approx. 2° in figure 5*e*). Given the flattened oval outlines of the organic membranes in horizontal sections (figure 5*a,b*), the change in orientation of the *c*-axes at the pointed-arched ends is very sudden and it is sometimes difficult to find CCRs with *c*-axes parallel to the elongation axis. This results in a 001 pole figure with two maxima aligned perpendicularly to the elongation axis (figure 5*a*). The 001 and 100 pole figures indicate that the CCRs' *c*-axes are co-oriented, whereas the *a*-axes are rotated. This can be qualified as a fibre texture. The low MUD values (18.14 in figure 5*a*) are indicative of a poor co-orientation. The map obtained on a vertical section (figure 5*c*) provides similar results, with CCRs' *c*-axes perpendicular to the growth lines, while their *a*-axes can take any orientation. Detailed maps centred on the internal organic membranes show that some individual CCRs may cross the membranes (figure 5*e,f*), although it is not possible to say if this is always the case.

In interlaminate figures (figure 6*a,b*), the elongated areas delineated by the primary septum and two consecutive denticles show consistent crystallographic patterns. They also show elongated CCRs similar to those found in the sheath, which converge from the edges of the septum and denticles towards the central axis, where we find CCRs parallel to this axis. These patterns can be compared to water flow in a drainage basin, in which the septum and denticles are the

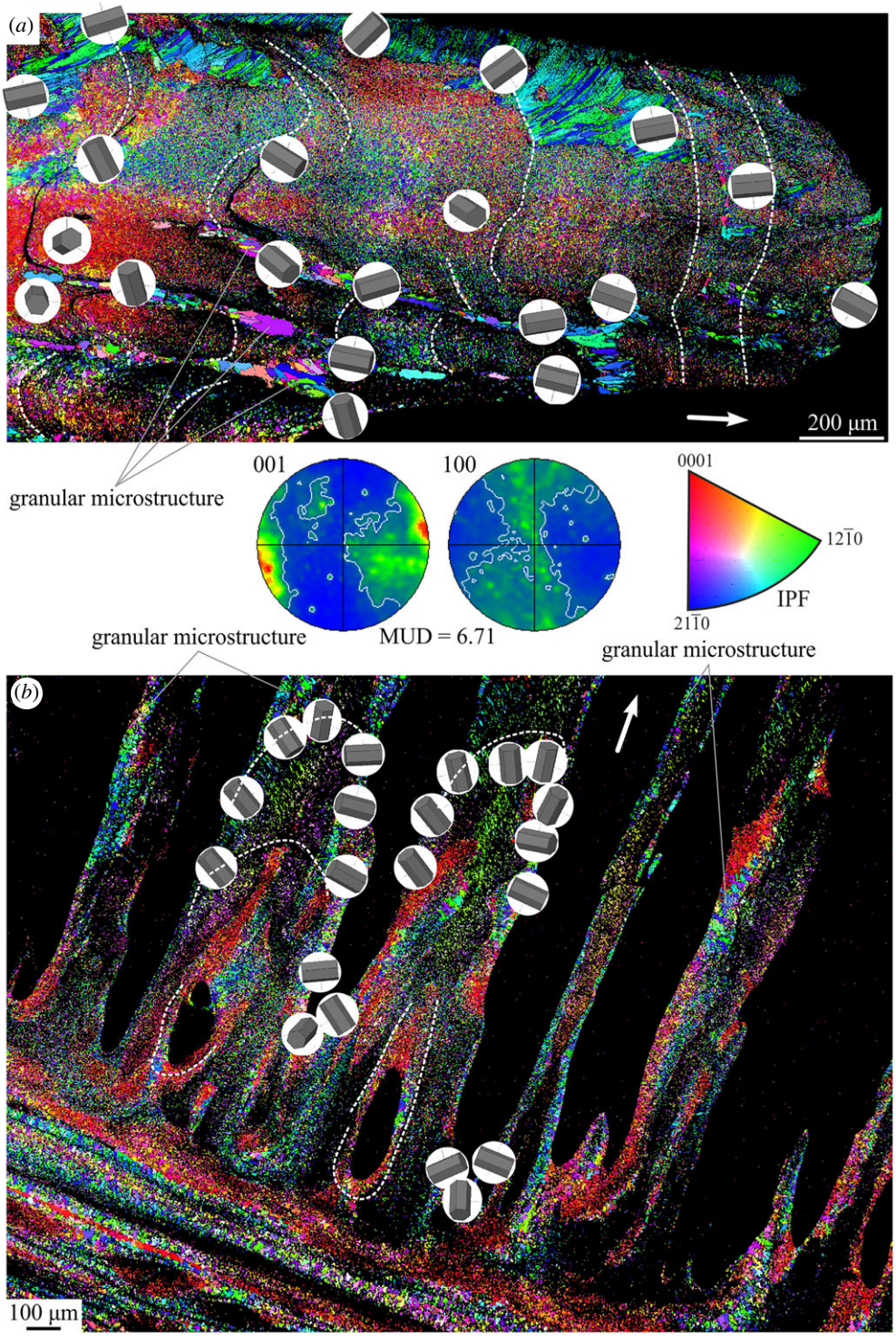

Figure 7. EBSD analysis of the radius. (*a*) Horizontal section. The 001 pole figure indicates a preferential orientation of the *c*-axes close to the overall growth direction of the radius (arrow), while the *a*-axes (100 pole figure) have no preferential orientation. (*b*) Vertical section. Growth lines in (*a*,*b*) have been estimated from the image quality maps (not shown). The unit cells have *c*-axes which are at high angles to the growth fronts (growth lines and edges of structures). The difference between the fibrous and granular microstructures is evident after the shape and size of CCRs. IPF, inverse pole figure (orientation colour key), valid for both maps.

most elevated parts and the central line is the river valley. When we plot the presumed distribution of growth lines (deduced from thin sections like those in figure 2*e*), it becomes clear that the elongated CCRs tend to align their *c*-axes perpendicularly to the growth lines (figure 6*b*,*c*). The high range of crystallographic orientations produces 001 and 100 pole figures with a high degree of scattering (figure 6*a*), and, accordingly, with low MUD values (5.52 in figure 6*a*). This wide range of crystallographic orientations fits in with the changing orientations of the CCRs described above. The very edges of the septum and denticles provided almost no indexable patterns, possibly due to the small crystallite size and the high organic content. The few indexed crystallites have *c*-axes which are at a very high angle to the surface (unit cells indicated with triangles in figure 6*b*,*c*).

A map on a horizontal section of a radius (figure 7*a*) reveals an alternation of blue–green and reddish bands elongated in the growth direction of the radius, which corresponds to areas where the *c*-axes change from being at a low angle to the image surface to a high angle. This is because the

section goes across dendrite branches similar to those in figure 4*i* and electronic supplementary material, figure S2, within which the orientation of fibres and their *c*-axes change drastically across small distances. The *c*-axes of the crystals in the blue–green CCRs are perpendicular or at a high angle to the growth lines. The small size of CCRs and the fibrous aspect of some blue–green CCRs (particularly abundant towards the top of figure 7*a*) are consistent with the fibrous nature of the material. Other areas made of granular microstructure show relatively wide CCRs with their *c*-axes aligned in the overall growth direction of the radius. They correspond to the sockets between crenulations (as in e.g. figure 2*h*). The 001 pole figures have two broad maxima oriented parallel to the overall growth direction of the radius, which marks the preferential orientation of the *c*-axes, whereas the distribution of the 100 figure indicates no preferential orientation for the *a*-axes. The general texture is very weak (MUD value = 6.71) and fibre-like (figure 7*a*). A similar pattern of alternation of reddish and bluish-to-greenish bands aligned in the growth direction of the radius is observed in the vertical section (figure 7*b*) for reasons similar to those above. Likewise, the small CCR size is also notable, and the crystals in a blue or green hue have *c*-axes which are at a high angle to the growth fronts. As in figure 7*a*, there are areas containing appreciably larger CCRs (i.e. granular microstructure), likely corresponding to the growth tracks of the crenulation sockets.

A longitudinal section of an ala has provided very few indexations (electronic supplementary material, figure S3), partly due to the small crystallite size. In any case, the crystallites have *c*-axes which are more or less in-plane and consistently at a high angle to the growth lines.

4. Discussion

The giant barnacle *A. psittacus* secretes a wall composed of six massive plates, plus a basal plate for attachment to the substrate. Despite the morphological complexity of the plates, particularly at their boundaries, the component microstructures are monotonic and consist of calcite grains, where the growth surface is in direct contact with the animal's soft tissue (most of the internal surfaces of plates), and thin calcite fibres, where the growth surfaces are in contact with acellular organic membranes (growth edges of radii and alae). The scutum of *Balanus amphitrite* (accepted as *Amphibalanus amphitrite*) is made of a seemingly identical granular microstructure [8]. In the growth surfaces of the granular microstructure, we observe grains in different stages of growth, some protruding above others by a matter of up to several micrometres (figure 4*a*,*c–e*), which suggests that the mantle is not able to level off the crystals in order to produce a smooth, even growth surface, as in, e.g. molluscs and brachiopods. Accordingly, the corresponding extrapallial space must be relatively wide and variable in thickness. This is unlike bivalves [18] and rhynchonelliform brachiopods [19], in which some microstructures are produced across extremely thin (100 nm or less) extrapallial spaces. Accordingly, the crystals can protrude only by a matter of tens of nanometres. The other microstructure secreted by balanids, the fibrous microstructure, displays smoother and more even growth surfaces (figure 4*g–i*; electronic supplementary material, figure S2). The growth fronts of these fibrous materials are attached to organic chitin-protein membranes, through which the mineral precursor components must diffuse to the mineralization sites [16]. In summary, these differences in microstructure can be traced back to differences in mineralization conditions, whether they are differences in the viscosity of the mineralization medium or the nature of the components (ions versus nanoaggregates, or the size of the latter).

The uniformity of microstructures makes it impossible to distinguish either layers (e.g. the internal layer [4]) or structures (e.g. paries versus sheath) based on the component units. These divisions have to be retained as purely morphological ones, and their boundaries are always imprecise.

Another remarkable aspect is the low degree of elaboration of microstructures, always reminiscent of inorganic calcite precipitates. In barnacles, the activity of the mantle cells seems restricted to delivering the necessary ingredients for crystal growth (calcium and carbonate ions, or amorphous calcium carbonate nanoaggregates) to the extrapallial space. This is again unlike other calcifiers, like molluscs or brachiopods, which are able to fabricate very sophisticated microstructures through a mixture of physical (self-organization processes) and biological (differential subcellular secretion, cellular contact recognition) processes [18]. Accordingly, the microstructural differences between barnacles and molluscs/brachiopods can be traced back to the secretory abilities of their mantles. In this sense, the barnacle mantle acts as a historical/phylogenetic restriction.

Despite the lack of biological control, the wall plates of *A. psittacus* display a certain degree of internal crystallographic organization. In particular, our SEM–EBSD results demonstrate that the microstructures are organized into bundles of evenly oriented grains or fibres (CCRs).

CCRs have irregular boundaries and elongate at a high angle or perpendicular to the growth lines. Their *c*-axes follow similar orientations. The latter data are consistent with previous X-ray diffraction data [6], although EBSD allows us to image crystal organization at the microscale. By comparing the extensions of CCRs (several tens of micrometres) and the sizes of grains (from less than one to a few micrometres), we conclude that the CCRs must be formed by many co-oriented calcite grains. CCRs clearly result from the epitaxial growth of calcite grains onto each other.

The development of a preferential orientation starting from more disorganized crystalline material in inorganic aggregates of columnar crystals can result from geometrical selection of crystals or competitive crystal growth [20,21]. In aggregates, where crystals have a common growth surface, crystals can only grow perpendicular to the substrate, where there is free space, such that lateral growth is inhibited. As a consequence, only those crystals oriented with their fastest growth direction (i.e. the *c*-axis in calcite) perpendicular to the growth front continue growing, while unfavourably oriented crystals will be intercepted and extinguished. This process results in the decrease in the number of crystals and the survivors progressively acquiring larger widths (at the expense of the victims) and common orientation (fibre texture). This process and the resulting microstructures are commonly observed in quartz geodes or druses, but also in metal ingot cast, which show microstructures similar to those observed here [22]. In calcified biomaterials, co-orientation by crystal competition has been invoked previously in the microstructures of some molluscs [23–25] and

in the avian eggshell [26,27]. An example of selection by competition within the shell of the cephalopod mollusc *Argonauta* is provided in electronic supplementary material, figure S4.

Conditions for competitive growth to occur in barnacles are also fulfilled since there is a directional supply of components needed for calcite growth (calcium and carbonate ions or amorphous calcium carbonate nanoaggregates, and organics) perpendicular to the growth front by the adjacent body epithelium. In addition, crystals have a common growth front lined by the calcifying epithelium, such that there must be competition for space. It is stressed that in barnacle wall plates, competition does not take place among individual crystals but among regions formed by crystals with a coherent orientation (the CCRs we define here). This competitive process explains the fast and sudden changes observed in the fibres composing the crenulations of the radius margins (figure 4*h*,*i*; electronic supplementary material, figure S2). In fibres, the axes of elongation are the *c*-axes and are clearly the fastest growth axes, as is frequent in calcite [28]. Nevertheless, in the granular microstructure, the grains are shapeless, rounded or rhombohedral, but do not particularly elongate along the *c*-axis. To explain the observed orientation, we can argue that grains pile up or nucleate onto each other preferentially in this direction. Growth would be of the epitaxial type, such that the crystallographic orientation will propagate across the CCR. Crystal clusters oriented with their *c*-axes perpendicular to the growth front would be favoured and continue growing, thus outcompeting other not so favourably oriented clusters. The process of competition can explain the irregular outlines of the CCRs, which may be further enhanced during epitaxial growth since it easily leads to lateral shifts due to differences in the position of the nucleation points (electronic supplementary material, figure S5). Accordingly, the crystallographic texture of the material results from purely physical laws, i.e. crystal growth.

It is interesting to note how some CCRs are able to go across the porous internal membranes periodically distributed within the plates (figure 5*e*,*f*). Most likely, some CCRs will stop at these obstacles, whereas others will appear de novo at the other side of the membranes. These membranes were previously attributed the responsibility for 'the organization of the shell mineral' by influencing 'the polymorphism, size, and orientation of shell-forming crystals' [29]. Although the origin of these membranes is still unknown, our data do not support their prevailing role in mineral growth and organization.

In their EBSD study on the alae of *Semibalanus balanoides*, Mitchell *et al*. [10] revealed areas of even orientations, which, in the absence of an SEM study, they interpreted as individual grains. Given their sizes, they are rather CCRs of the type recognized here. In agreement with our observations in *A. psittacus*, the CCRs of the alae of *S. balanoides* elongate and orient their *c*-axes perpendicular to the growth surfaces. These authors proposed a series of possible causes for this antimarginal orientation: (1) specific morphologies of calcite crystals, (2) age/growth stage of the organism, and (3) influence of the organic membranes existing at the tip of the ala. Cause (1) can be discarded since we have found similar crystallographic textures in both the granular and fibrous microstructures. Cause (2) was based on the recognition of another, more finely textured material away from the ala margin, which they interpreted as corresponding to different growth stages, whereas the more internal material might well correspond to the paries or sheath, with a granular texture and different crystallographic orientation. Regarding cause (3), organic membranes might well determine the orientations of fibres of alae and radii, but only at the positions where the growth margin is in direct contact with them, i.e. the crests, but not at the troughs (figure 4*h*,*i*). Nevertheless, the orientation patterns with the *c*-axes of crystals perpendicular to the growth surface are the same throughout the whole growth surfaces. In other instances (the basal growth surfaces of plate paries), there are no detectable organic membranes, which could perform a crystal-orientation function.

Our study is the first one in which the crystallographic pattern of organization is revealed in a barnacle, and our conclusions can be extended to, at least, balanoids. Although some comprehensive work was carried out by Bourget [4,5] on sessilian barnacles, the range of microstructures and their organization in barnacles should be reexamined and expanded with new high-resolution morphological and crystallographic characterization techniques.

An account of the diversity of microstructures of cirripeds and of their organization is essential with regard to the phylogeny of the group, but also to other kinds of studies for which cirripeds are important or essential study subjects, such as bioadhesion materials, biofouling and vulnerability to ocean acidification.

Data accessibility. Data have been uploaded as part of the electronic supplementary material, figures S1–S5.

Authors' contributions. A.G.C. conceived and designed the study, analysed data and wrote the paper. A.G.-S. acquired and analysed data and revised the paper. A.B.R.-N. revised the paper for important intellectual content. N.A.L. conceived and designed the study, revised the paper.

Competing interests. We declare we have no competing interests.

Funding. This research was funded by projects CGL2017-85118-P (A.G.C., A.G.-S.) and CGL2015-64683-P (A.B.R.-N.) of the Spanish Ministerio de Ciencia e Innovación, the Unidad Científica de Excelencia UCE-PP2016-05 of the University of Granada (A.G.C., A.B.R.-N.) and the Research Group RNM363 of the Junta de Andalucía (A.G.C.). N.A.L., A.G.C. and A.B.R.-N. acknowledge support from CONICYT-Chile through grant nos. FONDECYT 1140938, PCI REDES 170106 and PIA ANILLOS ACT172037, for international collaborative research.

References

1. Lagos NA, Castilla JC, Broitman B. 2008 Spatial environmental correlates of intertidal recruitment: a test using barnacles in northern Chile. *Ecol. Monogr.* **78**, 245–261. (doi:10.1890/07-0041.1)
2. Holm ER. 2012 Barnacles and biofouling. *Integr. Comp. Biol.* **52**, 348–355. (doi:10.1093/icb/ics042)
3. Pitombo FB. 2004 Phylogenetic analysis of the Balanidae (Cirripedia, Balanomorpha). *Zool. Scripta* **33**, 261–276. (doi:10.1111/j.0300-3256.2004.00145.x)
4. Bourget E. 1977 Shell structure in sessile barnacles. *Natur. Can.* **104**, 281–322.
5. Bourget E. 1987 Barnacle shells: composition, structure, and growth. In *Crustacean issues: barnacle biology*, vol. 5 (ed. AJ Southward), pp. 267–285. Rotterdam, The Netherlands: A. A. Balkema.
6. Rodríguez-Navarro AB *et al.* 2006 Microstructure and crystallographic-texture of giant barnacle

(*Austromegabalanus psittacus*) shell. *J. Struct. Biol.* **156**, 355–362. (doi:10.1016/j.jsb.2006.04.009)

7. Wang X, Xiao Y, Wang C, Niu J, Ma J, Wang H, Li X, Chen X, Huang F. 2017 Hierarchical interfacial structuring of the calcareous base of the barnacle *Balanus albicostatus* over different length scales. *Mater. Chem. Phys.* **192**, 48–57 (doi:10.1016/j.matchemphys.2017.01.053)
8. Khalifa GM, Weiner S, Addadi L. 2011 Mineral and matrix components of the operculum and shell of the barnacle *Balanus amphitrite*: calcite crystal growth in a hydrogel. *Cryst. Growth Des.* **11**, 5122—5130. (doi:10.1021/cg2010216)
9. Lewis AC, Burden DK, Wahl KJ, Everett RK. 2014 Electron backscatter diffraction (EBSD) study of the structure and crystallography of the barnacle *Balanus amphitrite*. *JOM* **66**, 143–148. (doi:10.1007/s11837-013-0793-y)
10. Mitchell RL, Coleman M, Davies P, North L, Pope EC, Pleydell-Pearce C, Harris W, Johnston R. 2019 Macro-to-nanoscale investigation of wall-plate joints in the acorn barnacle *Semibalanus balanoides*: correlative imaging, biological form and function, and bioinspiration. *J. R. Soc. Interface* **16**, 20190218. (doi:10.1098/rsif.2019.0218)
11. Griesshaber E, Yin X, Ziegler A, Checa A, Eisenhauer A, Schmahl WW. 2017 Patterns of mineral organization in carbonate biological hard materials. In *Highlights in applied mineralogy* (eds S Heuss-Aßbichler, G Amthauer, M John), pp. 245–272. Berlin, Germany: De Gruyter.
12. Newman WA, Zullo VA, Wainwright WA. 1967 A critique on recent concepts of growth in Balanomorpha (Cirripedia, Thoracica). *Crustaceana* **12**, 167–178. (doi:10.1163/156854067X00594)
13. Newman WA, Zullo VA, Withers TH. 1969 Cirripedia. In *Treatise on invertebrate paleontology, part R, Arthropoda* (ed. RC Moore), pp. R206–R295. Lawrence, KS: Geological Society of America and Kansas University Press.
14. Pitombo FB. 1999 Comparative morphology of the Balanidae (Cirripedia): a primer to a phylogenetic analysis. In *Crustaceans and the biodiversity crisis: Proceedings of the Fourth International Crustacean Congress* (eds FR Schran, JC von Vaupel Klein), pp. 151–171. Leiden, The Netherlands: Brill.
15. Gale AS, Sørensen AM. 2014 Origin of the balanomorph barnacles (Crustacea, Cirripedia, Thoracica): new evidence from the Late Cretaceous (Campanian) of Sweden. *J. Syst. Paleontol.* **13**, 791–824. (doi:10.1080/14772019.2014.954824)
16. Checa AG, Salas C, Rodríguez-Navarro AB, Grenier C, Lagos NA. 2019 Articulation and growth of skeletal elements in balanid barnacles (Balanidae, Balanomorpha, Cirripedia). *R. Soc. open sci.* **6**, 190458. (doi:10.1098/rsos.190458)
17. Dauphin Y. 2008 The nanostructural unity of mollusc shells. *Miner. Mag.* **72**, 243–246. (doi:10.1180/minmag.2008.072.1.243)
18. Checa A. 2018 Physical and biological determinants of the fabrication of molluscan shell microstructures. *Front. Mar. Sci.* **5**, 353. (doi:10.3389/fmars.2018.00353)
19. Simonet RM *et al.* 2019 Calcite fibre formation in modern brachiopod shells. *Sci. Rep.* **9**, 598. (doi:10.1038/s41598-018-36959-z)
20. Grigor'ev DP. 1965 *Ontogeny of minerals*. Jerusalem, Israel: Israel Program for Scientic Translations.
21. Rodríguez-Navarro AB. 2001 Model of texture development in polycrystalline films growing on amorphous substrates with different topographies. *Thin Solid Films* **389**, 288–295. (doi:10.1016/s0040-6090(01)00863-x)
22. Stefanescu DM, Ruxanda R. 2004 Solidification structure of aluminum alloys. In *ASM handbook vol. 9: metallography and microstructures* (ed. GF Vander Voort), pp. 107–115. Novelty, OH: ASM International.
23. Ubukata T. 1994 Architectural constraints on the morphogenesis of prismatic structure in Bivalvia. *Palaeontology* **37**, 241–261.
24. Checa AG, Rodríguez-Navarro A. 2001 Geometrical and crystallographic constraints determine the self-organization of shell microstructures in Unionidae (Bivalvia: Mollusca). *Proc. R. Soc. B* **268**, 771–778. (doi:10.1098/rspb.2000.1415)
25. Stevens K, Griesshaber E, Schmahl W, Casella LA, Iba Y, Mutterlose J. 2017 Belemnite biomineralization, development, and geochemistry: the complex rostrum of *Neohibolites minimus*. *Palaeogeogr. Palaeoclimatol. Palaeoecol.* **468**, 388–402. (doi:10.1016/j.palaeo.2016.12.022)
26. García-Ruiz JM, Rodríguez-Navarro A, Kälin O. 1995 Textural analysis of eggshells. *Mater. Sci. Eng. C* **3**, 95–100. (doi:10.1016/0928-4931(95)00107-7)
27. Rodríguez-Navarro A, García-Ruiz JM. 2000 Model of textural development of layered crystal aggregates. *Eur. J. Mineral.* **12**, 609–614. (doi:10.1127/0935-1221/2000/0012/0609)
28. Rodríguez-Navarro AB, Yebra A, Nys Y, Jiménez-López C, García-Ruiz JM. 2007 Analysis of avian eggshell microstructure using X-ray area detectors. *Eur. J. Mineral.* **19**, 391–398. (doi:10.112710935-1221/2007/0019-1724)
29. Fernández MS, Arias JI, Neira-Carrillo A, Arias JL. 2015 *Austromegabalanus psittacus* barnacle shell structure and proteoglycan localization and functionality. *J. Struct. Biol.* **191**, 263–271. (doi:10.1016/j.jsb.2015.08.005)